Manuscript prepared for Biogeosciences
with version 5.0 of the LaTeX class copernicus.cls.
Date: 21 January 2015

Frozen ponds: production and storage of methane during the Arctic winter in a lowland tundra landscape in northern Siberia, Lena River Delta

M. Langer[1], S. Westermann[2,3], K. Walter Anthony[4], K. Wischnewski[1], and J. Boike[1]

[1]Alfred-Wegener-Institut Helmholtz-Zentrum für Polar- und Meeresforschung, Periglacial Research Section, Potsdam, Germany
[2]University of Oslo, Department of Geography, Oslo, Norway
[3]Center for Permafrost (CENPERM), Department of Geosciences and Natural Resource Management, University of Copenhagen, Copenhagen, Denmark
[4]University of Alaska Fairbanks, Water and Environmental Research Center, Fairbanks, USA

Correspondence to: Moritz Langer
(moritz.langer@awi.de)

Abstract. Lakes and ponds play a key role in the carbon cycle of permafrost ecosystems, where they are considered to be hotspots of carbon dioxide CO_2 and methane CH_4 emission. The strength of these emissions is, however, controlled by a variety of physical and biogeochemical processes whose responses to a warming climate are complex and only poorly understood. Small waterbodies have been attracting an increasing amount of attention since recent studies demonstrated that ponds can make a significant contribution to the CO_2 and CH_4 emissions of tundra ecosystems. Waterbodies also have a marked effect on the thermal state of the surrounding permafrost; during the freezing period they prolong the period of time during which thawed soil material is available for microbial decomposition.

This study presents net CH_4 production rates during the freezing period from ponds within a typical lowland tundra landscape in northern Siberia. Rate estimations were based on CH_4 concentrations measured in surface lake ice from a variety of waterbody types. Vertical profiles along ice blocks showed an exponential increase in CH_4 concentration with depth. These CH_4 profiles were reproduced by a 1D mass balance model and the net CH_4 production rates were then inferred through inverse modeling.

Results revealed marked differences in early winter net CH_4 production among various ponds. Ponds situated within intact polygonal ground structures yielded low net production rates, of the order of 10^{-11} to $10^{-10}\,\mathrm{mol\,m^{-2}\,s^{-1}}$ (0.01 to $0.14\,\mathrm{mg_{CH_4}\,m^{-2}\,d^{-1}}$). In contrast, ponds exhibiting clear signs of erosion yielded net CH_4 production rates of the order of $10^{-7}\,\mathrm{mol\,m^{-2}\,s^{-1}}$ ($140\,\mathrm{mg_{CH_4}\,m^{-2}\,d^{-1}}$). Our results therefore indicate that, once a particular threshold in thermal erosion has been crossed, ponds can develop into major CH_4 sources. This implies that any future warming of the climate may result in non-linear CH_4 emission behavior in tundra ecosystems.

1 Introduction

Up to 28% of the land surface in permafrost landscapes has been attributed to lakes and ponds (Emmerton et al., 2007; Grosse et al., 2008; Muster et al., 2013). Several studies have emphasized that waterbodies are fundamental elements in Arctic ecosystems and exert a strong control on the Arctic heat, water, and carbon cycle (Cole et al., 2007; McGuire et al., 2009). This is especially true in permafrost landscapes, where large quantities of carbon are trapped in the frozen soils that can surround waterbodies (e.g. Hugelius et al., 2013). Any future mobilization and emission of the old carbon pool is likely to result in a positive feedback to global warming (O'Connor et al., 2010; Koven et al., 2011).

Lakes are considered to play a key role in the turnover and emission of the carbon in these permafrost reservoirs (Boike et al., 2012). Many of the studies to date have focused on the greenhouse gas emission potential of large lakes such as thermokarst lakes (Zimov et al., 1997; Walter et al., 2006;

Brosius et al., 2012). However, recent studies have demonstrated that not only large Arctic lakes, but also the smaller Arctic ponds, are hotspots of CO_2 and CH_4 emission (Abnizova et al., 2012; Laurion et al., 2010). In lowland tundra landscapes such as the Lena River Delta, more than 30% of the total inland water surface can be attributed to waterbodies with surface areas less than $1\,\mathrm{km}^2$ (Muster et al., 2012). Most of the studies to date addressing greenhouse gas emissions from Arctic ponds have focused on the summer months, but a considerable carbon turnover is also possible in waterbodies during the freezing period, until the bottom sediments are completely frozen (Karlsson et al., 2013). During winter the closed ice cover inhibits the diffusion of oxygen into the water which strongly limits the oxidation of CH_4 in the water column. Several studies have demonstrated that large quantities of CH_4 are produced during the long-lasting winter period and stored in the form of bubbles within the ice cover (Walter Anthony et al., 2010; Wik et al., 2011; Boereboom et al., 2012; Walter Anthony and Anthony, 2013).

Bubbles trapped in lake ice, resulting from a number of different processes, include ebullition bubbles, bubbles from freeze-degassing of dissolved gases, and photosynthesis bubbles. These can usually be distinguished from each other on the basis of their size, morphology, and gas content (Boereboom et al., 2012; Walter Anthony and Anthony, 2013). This study focuses on CH_4 which is stored in the form of bubbles from freeze-degassing which are continuously formed at the advancing freezing front and occur in closely spaced layers in the ice cover (Lipp et al., 1987). Due to freeze-degassing dissolved gases enrich in a very thin water layer directly at the freezing front. The saturation of dissolved gases in this thin water layer leads to bubble nucleation. The gas concentration in the growing bubbles is in equilibrium with the dissolved gases of the surrounding water (Wei et al., 2003). As soon as the bubbles are completely entrapped within the ice cover they are sealed from further gaseous exchange so that an enrichment of dissolved gases and bubble nucleation at the freezing front starts again. This results in continuous formation of freeze-out bubble layers which preserve to a certain degree information about the concentration of the dissolved gases in the water column during the time of freezing (Lipp et al., 1987; Craig et al., 1992; Killawee et al., 1998). The frequency of bubble layer formation, bubble size, and bubble shape are largely dependent on the rate of freezing (Carte, 1961; Yoshimura et al., 2008). The sizes of freeze-out bubbles are reported to range between micrometers to millimeters at natural freezing rates of the order of millimeters per day (Lipp et al., 1987; Yoshimura et al., 2008).

The storage of CH_4 within the ice cover of shallow Alaskan lakes has been investigated by Phelps et al. (1998). They found that CH_4 concentrations were very low in the upper part of the ice cover, but increased rapidly with depth. This behavior was explained by supersaturation of dissolved gases due to the shrinking volume of available water underneath the growing ice cover. In addition, the concentration of dissolved CH_4 was observed to increase at the water-ice interface over the winter period. However, it remains unclear whether this CH_4 accumulation in the shrinking water column was caused by freeze-degassing of CH_4, ongoing CH_4 production during ice cover formation, or a combination of both. In addition, Phelps et al. (1998) also found that the CH_4 stored in the ice cover was largely released into the atmosphere during spring melt. Furthermore, they were able to show that the amount of CH_4 emitted in spring equated to half of the total annual CH_4 emissions from the lake. These results served to further stress the importance of the freezing period to the carbon cycle of tundra-lake ecosystems.

In this study we present profiles derived from measurements of CH_4 concentrations in the ice cover of nine typical Arctic ponds and lakes in the Lena River Delta of north-eastern Siberia. An extensive survey of pond areas and depths has provided insights into the development stages of the various waterbodies within the area of investigation. Temperature profiles were derived from measurements in three different ponds and used to investigate their freezing behavior. A 1D mass balance model was developed to reconstruct the storage of CH_4 within the ice cover and the CH_4 concentration profiles (derived from CH_4 concentration measurements in the ice cover) were used to infer net CH_4 production rates during the freezing period by inverse modeling. For the first time, this allows to distinguish between CH_4 accumulation caused by freeze-degassing and ongoing CH_4 production during freeze-up.

2 Study area

The study area is located in the Lena River Delta of north-eastern Siberia, within the zone of continuous permafrost (Fig. 1). The region is characterized by an Arctic continental climate with a mean annual air temperature of about $-14^\circ\,\mathrm{C}$. Winter temperatures frequently fall below $-45^\circ\,\mathrm{C}$ while summer temperatures can exceed $25^\circ\,\mathrm{C}$ (Langer et al., 2011a; Boike et al., 2013). The cold climate results in very cold permafrost temperatures: an annual average temperature of about $-9^\circ\,\mathrm{C}$ has been recorded at a depth of $27\,\mathrm{m}$ (Boike et al., 2013). Permafrost in the Lena River Delta region is reported to extend to depths of several hundred meters (Grigoriev, 1960). The study area is located on Samoylov Island in the central part of the Lena River Delta ($72^\circ\,22'\mathrm{,N},\ 126^\circ\,28'\mathrm{E}$). The Island is mainly characterized by a Holocene cryogenic soil complex that is largely characterized by the typical micro-relief of polygonal patterned ground formed by frost cracking and subsequent ice-wedge formation (Lachenbruch, 1962). The polygonal structures usually consist of depressed, water-saturated centers surrounded by elevated rims. The soil in the polygonal centers usually consists of sandy peat while the elevated rims are usually covered with a dry moss layer underlain by wet sandy peat soils and massive ice wedges (Kutzbach et al., 2004).

The gravimetric content of soil organic carbon was measured to range from about 1 to 24% at the study site (Zubrzycki et al., 2013). The polygonal ground structures are present in different stages of degradation. Ponding water is often found in the depressed polygon centers (intra-polygonal ponds) or along the troughs between the polygon rims above the ice-wedges (ice-wedge ponds) (Fig. 2 a, b) (Wetterich et al., 2008; Helbig et al., 2013; Negandhi et al., 2013). Both intra-polygonal ponds and ice-wedge ponds are usually very shallow, with water depths ranging from just a few centimeters to a few tens of centimeters. Such ponds often feature emergent vegetation, consisting mainly of hydrophilic species such as *Carex aquatilis* and such as mosses *Scorpidium scorpioides* (Kutzbach et al., 2007; Liebner et al., 2011). The rims surrounding intra-polygonal ponds are mostly intact with little or no sign of degradation. However, degradation of the polygonal structures can result in ponds merging to form larger ponds that often consist of several polygons, typically showing clear signs of degradation (Fig. 2 c) (Helbig et al., 2013). They feature open water surfaces and lack emergent vegetation in their centers. The study area is also characterized by thermokarst (thaw) lakes, which are a result of advanced permafrost degradation associated with further thermal erosion processes (Morgenstern et al., 2013). About 50% of the free water surface on Samoylov Island is attributed to ponds, with the remaining 50% attributed to lakes, including both thermokarst lakes and oxbow lakes (Muster et al., 2012).

3 Methods and materials

3.1 Pond survey and classification

The distribution and sizes of waterbodies within the study area were mapped using ortho-rectified, visual and near-infrared aerial images. The study area (SA) lies on the first terrace of Samoylov Island and covers a typical wet lowland tundra landscape; it has a surface area of about $1.5\,\mathrm{km}^2$ (Fig. 1). We used the supervised surface water classification from Muster et al. (2012) to extract a size distribution for the ponds and lakes within the area. Water depth measurements were also collected from two sub-areas (SUB I and SUB II), each of which had a surface area of about $30000\,\mathrm{m}^2$ (Fig. 1). The water depths were measured manually using a depth sounder, or using a ruler where the water levels were very low.

In this study we mainly focused on small waterbodies (ponds) smaller than $10000\,\mathrm{m}^2$. On the basis of morphology we distinguish between ice-wedge ponds (Fig. 2 a), intra-polygonal ponds (Fig. 2 a), and merged ponds (Fig. 2 c). These ponds are further grouped into initial state ponds (ISPs) and advanced state ponds (ASPs) according to the degrees of degradation of the polygonal ground structures within which the ponds occur. ISPs are defined as ponds that occur within almost intact polygonal structures; they include both ice-wedge ponds located between polygon rims (Fig. 2a) and intra-polygonal ponds located in polygon centers (Fig. 2b). ISPs are shallow with water depths of less than $0.5\,\mathrm{m}$. Their horizontal extent typically ranges from a few meters up to about $10\,\mathrm{m}$, which is a typical diameter for the polygonal structures. Due to initial degradation ISPs can be hydrologically interconnected with other ISPs or with larger waterbodies, but the individual polygon shape is still preserved. In contrast, ASPs show clear signs of degradation in the surrounding polygonal tundra (Fig. 2c). The center of an ASP is much deeper due to thaw settlement in the underlying bottom sediments, so that ASPs usually have water depths greater than $0.5\,\mathrm{m}$. ASPs typically range in diameter from about 10 to $50\,\mathrm{m}$. Waterbodies that reach depths greater than $2\,\mathrm{m}$ are likely to remain unfrozen at the bottom throughout the winter, and a continuously unfrozen layer (talik) then develops in the sediments. These deeper waterbodies are usually larger with horizontal extent ranging from about $50\,\mathrm{m}$ to several hundreds of meters. Therefore, these waterbodies are classified as lakes. At the study site these lakes occur either in the form of oxbow lakes or thermokarst lakes which can be distinguished according to multiple geomorphological indicators such as shape and location. Oxbow lakes were excluded from this study. ISPs, ASPs, and thermokarst lakes can be part of an evolutionary process of permafrost degradation so that transitional forms between these waterbody types exist.

3.2 Monitoring ice cover formation

The process of ice cover formation was observed through three temperature profiles obtained from three different ponds. The temperatures were recorded using water temperature loggers (Onset, HOBO Pro v2 with an accuracy of better than $\pm 0.5^\circ\,\mathrm{C}$) positioned along a metal wire hanging down from a small buoy anchored in the middle of each pond. The first temperature profile was from an intra-polygonal pond, based on measurements from four temperature sensors. The first three temperature sensors were installed at depths of $0\,\mathrm{m}$, $0.15\,\mathrm{m}$, and $0.33\,\mathrm{m}$. The lowermost sensor was fixed directly on the ground at a depth of $0.4\,\mathrm{m}$. The pond was transitional between ISPs and ASPs in its level of degradation. Temperature profiles were also obtained for two typical ASPs, in each case using six temperature sensors over a depth of about $0.8\,\mathrm{m}$. In ASP1 the temperature sensors were deployed at depths of $0\,\mathrm{m}$, $0.20\,\mathrm{m}$, $0.35\,\mathrm{m}$, $0.53\,\mathrm{m}$, $0.67\,\mathrm{m}$, and $0.76\,\mathrm{m}$. In ASP2 the sensors were deployed at depths of $0\,\mathrm{m}$, $0.20\,\mathrm{m}$, $0.33\,\mathrm{m}$, $0.50\,\mathrm{m}$, $0.71\,\mathrm{m}$, and $0.75\,\mathrm{m}$. With exception of the lowermost sensors which were fixed to the ground, all sensors were hold in place relative to the water surface by the floating buoy.

The ice cover thickness in each pond was inferred using the temperature records from the individual sensors. The date on which the freezing front crossed the temperature sensor was

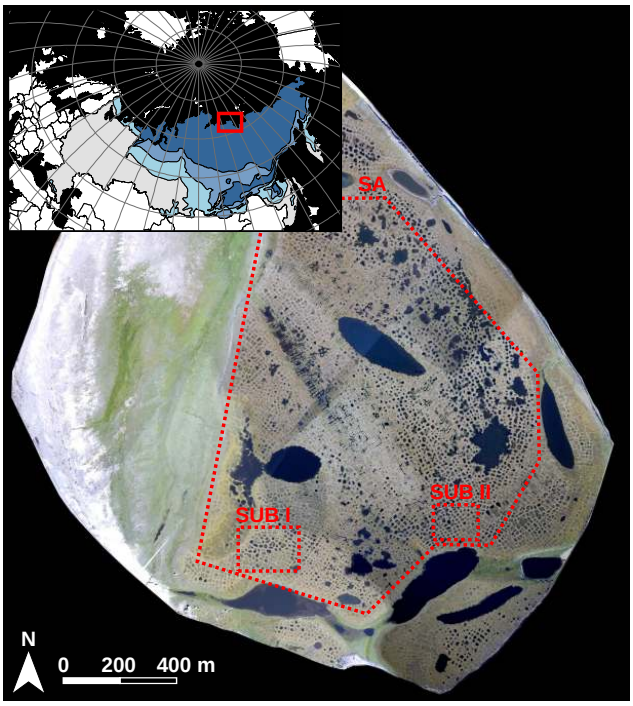

Fig. 1. Location of the study area in northern Siberia within the zone of continuous permafrost (a) (map after: Brown et al., 1997), and ortho-rectified aerial image of Samoylov Island (b). The main study area (SA) and the two sub-areas (SUB I, SUB II) used for the pond and lake mapping and for sampling are outlined in red.

identified by a sudden drop in temperature after a relatively long period at a constant temperature of $0°\,\mathrm{C}$.

3.3 Sampling methane concentrations in lake ice

Thirteen CH_4 concentration profiles were obtained from ice blocks cut from eight waterbodies using a chainsaw (STIHL, Germany) with a $40\,\mathrm{cm}$ guide bar during a field program in April 2011. Three waterbodies were ponds with maximum water depths of less than $0.5\,\mathrm{m}$. The morphology of these ponds still placed them within the ISP category, despite some early signs of degradation. In the following, these ponds are named ISP1, ISP2, and ISP3. Four waterbodies had maximum depths greater than $0.5\,\mathrm{m}$ (up to $1.2\,\mathrm{m}$) and occurred within clearly degraded polygonal ground structures. The four ponds fell into the ASP category and are named ASP1 to ASP4 in the following. One of the sampled waterbodies fell into the category of a thermokarst lake with a maximum water depth of $5.3\,\mathrm{m}$. Temperature chains were installed in ISP1, ASP1, and ASP2 in order to observe ice cover growth (see Sect. 3.2). Despite the limited number of samples, the eight waterbodies provide a good cross-section through the different types of ponds and lakes at the study site.

The ice blocks were extracted by cutting ice columns to a depth of about $35\,\mathrm{cm}$, with surface dimensions of about $20\,\mathrm{cm}$ by $30\,\mathrm{cm}$, from the ice cover. A second ice column was then cut below the hole left by the first column in order to obtain ice profiles down to a maximum depth of about $70\,\mathrm{cm}$. The ice columns were cut into smaller cuboids with a base area of about $7 \times 7\,\mathrm{cm}$ and a height of $10\,\mathrm{cm}$. The cuboids were cleaned with a sharp and sterilized knife prior to transportation and analysis.

The ice samples were melted in $1\,\mathrm{l}$ plastic containers (Nalgene, USA), which were sealed with PTFE paste (Äronix, Germany). The impermeability of the containers to gas was verified by long-term testing using calibration gases prior to the analyses. The containers were flushed with nitrogen immediately after sealing in order to ensure zero CH_4 concentration in the head space prior to melting. The head space volume in the containers varied between 0.3 and $0.6\,\mathrm{l}$ according to differences in sample volume. Possible corruption of the CH_4 concentration measurements due to microbial activity during the melt procedure was tested using acidified (10% HCL) parallel samples, but these showed no significant differences in CH_4 concentration from the pure samples. Methane concentrations within the ice samples were determined by gas chromatography at the field station on Samoylov Island, using an Agilent GC 7890 gas chromatograph (Agilent Technologies, Germany) equipped with a Porapak Q column ($1.8\,\mathrm{m}$ length, $2\,\mathrm{mm}$ ID) and a flame ionization detector (FID). Four repeat concentration measurements (five measurements in total) were performed in order to determine the measurement uncertainty.

The total CH_4 content in the ice samples was evaluated by taking into account the head space concentration, sample volume, temperature, and pressure. A correction was also made for dissolved CH_4 in the melt water using Henry's law. These procedures introduced a wide range of potential error sources into the CH_4 content measurements. Thus, the uncertainties in the total CH_4 content were determined by Monte-Carlo simulations assuming uniform uncertainty distributions for all parameters including measurement uncertainty, head space volume, sample volume, ambient temperature, and pressure (e.g. Anderson, 1976).

3.4 Modeling methane concentrations in the ice cover of ponds

The storage of methane in the ice cover of ponds was simulated using a simplified 1D mass balance scheme, in an approach that closely resembles that used by Boereboom et al. (2012). The model was used to calculate net CH_4 production rates during the freezing process by fitting the model to the CH_4 concentration profiles obtained from the ice cover. The model simulated an ice cover growing downwards from the surface to the bottom of the pond, assuming a constant accumulation of bubbles from freeze-degassing of dissolved gases at the ice-water interface (see Appendix A). Ebullition bubbles were not taken into account in the model. Despite

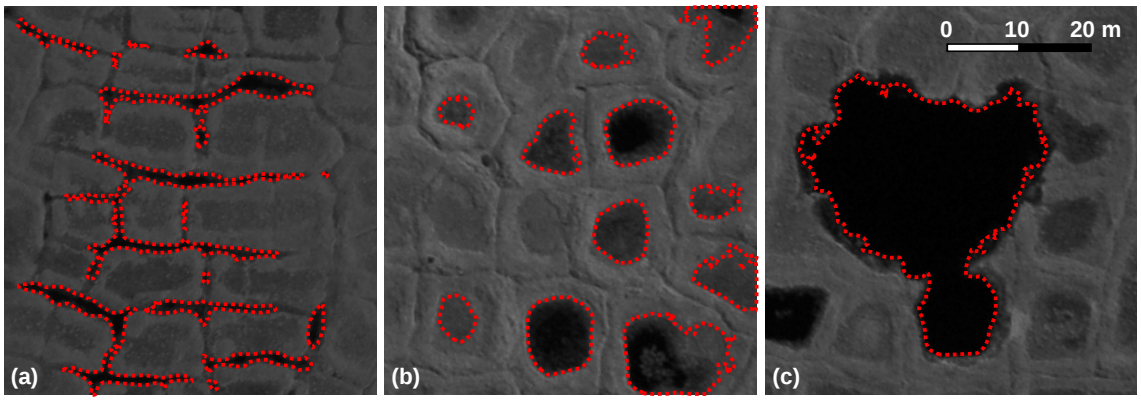

Fig. 2. Typical ponds in the polygonal tundra mapped from near infrared (NIR) areal images. At the study site occur (a) ice-wedge ponds, (b) intra-polygonal ponds within intact polygonal structures, and (c) merged ponds show clear signs of degradation of the polygonal structures. According to their degree of degradation intra-polygonal ponds and ice-wedge ponds are classified as initial state ponds (ISPs) and merged ponds as advanced state ponds (ASPs).

their importance as an efficient mode of CH_4 emission from lakes, ebullition bubbles have small diameters relative to the lake surface area and they usually have a rare and heterogeneous distribution within a thermokarst pond, making them difficult to quantify from a limited number of small ice samples (Walter Anthony and Anthony, 2013). The heterogeneous distribution of ebullition bubbles also means that they are impossible to simulate using a simplified 1D mass balance scheme. This limitation of the model means that the CH_4 storage, and hence the production of CH_4 in ponds, tends to be underestimated. The model results can therefore be considered to be conservative when calculating net CH_4 production rates. Since the size of bubbles from freeze-degassing depends largely on the rate of freezing (Carte, 1961), we assumed that the accumulation of freeze-out bubbles was adequately represented by a constant rate during periods of constant freezing (Yoshimura et al., 2008).

The partial pressure of CH_4 in the bubbles was assumed to be always in equilibrium with the partial pressure of CH_4 in the water column, following Henry's law. The CH_4 enrichment (net CH_4 production) is controlled by CH_4 production and oxidation. Very stable temperature conditions with slowly decreasing temperatures from about 2 to $0°\,C$ were observed at the bottom of shallow ponds and lakes during the freezing period from October through February at the study site (Boike et al., 2013). Assuming a standard Q_{10} relation between CH_4 production and temperature ($Q_{10} = 3$), a maximum change in net CH_4 production of about a factor of 1.3 can be expected (Van Hulzen et al., 1999). Thus, we assumed constant CH_4 production and oxidation rates during the freezing period. Furthermore, other factors controlling CH_4 production such as sediment composition are assumed to remain constant during the freezing period. We also assumed a uniform enrichment of methane in the water column beneath the ice cover. A uniform distribution of dissolved CH_4 in the shrinking water column is considered a reasonable guess for the investigated very shallow waterbodies albeit concentration gradients are reported for deeper lakes. However, increased CH_4 concentrations at the bottom of the ponds would lead to underestimated net CH_4 production in the model calculations. As well as the stable temperature conditions, the model also assumed constant pressure conditions during the freezing process. Nevertheless, air pressure changes are an important factor for bubble formation in lakes and can result in layers of dense bubbles in the ice cover (Walter Anthony et al., 2010). Thus, the obtained ice profiles were analyzed for occurrence of bubble layers that were related to air pressure changes before they were used for modeling. The storage of bubbles in the ice cover was simulated by integrating an effective bubble cross-section and CH_4 concentration over the current ice cover thickness. The effective bubble cross-section was calculated as horizontal area occupied by bubbles of an infinitesimal thin horizontal ice cover slices with an area of $1\,m^2$. The bubble volume stored in the ice cover was assumed to be no longer in gaseous exchange with the unfrozen waterbody. When the maximum solubility of methane in the shrinking water column was reached the model assumed that the excess methane was stored directly in the ice cover. The storage of excess CH_4 resulted in a marked increase in the methane concentration within the ice cover.

The mass balance scheme results in a first order ordinary differential equation, which can be solved analytically (see Appendix A). In general, the model outcome is determined by the net CH_4 production rate, the effective bubble cross-section, the ice cover growth rate, and the pond depth. The pond depth and the ice cover growth rate are measured and hence known for all sites, and the net CH_4 production rate

and effective bubble cross-section can be inferred by fitting the model to measured CH_4 concentration profiles. Previous measurements within the study area have shown that the concentration of dissolved CH_4 in different ponds varies widely (between 6×10^{-9} and $2 \times 10^{-5}\,\mathrm{mol\,m^{-3}}$) prior to the onset of freezing (Abnizova et al., 2012). The sensitivity of the fitting procedure was therefore tested over the entire range of initial CH_4 concentrations. The model was fitted to the measured CH_4 profiles from the ice samples using a non-linear fitting routine provided by MATLAB. This fitting procedure included evaluation of the 95% confidence intervals on the fitted parameters and the model output.

4 Results

4.1 Waterbody distribution and ice cover formation

Almost 15% of the study area (SA) consists of waterbodies, of which about 60% are less than $300\,\mathrm{m^2}$ in surface area (Fig. 3a). In the sub-areas SUB I and SUB II the pond surface areas range between 0 and $300\,\mathrm{m^2}$ and the maximum water depth ranges between 0 and $1.5\,\mathrm{m}$. About 10% of the tundra landscapes in SUB I and SUB II are occupied by ponds that are shallower than $0.2\,\mathrm{m}$. Most of these shallow ponds fall into the ISP class, with little or no sign of degradation in the surrounding polygon rims. Ponds with water depths of 0.5 to 0.6 m and 0.8 to 1.0 m were found to be slightly more abundant than ponds with water depths of 0.2 to $0.4\,\mathrm{m}$ and 1.0 to $1.3\,\mathrm{m}$ (Fig. 3b). Most of the ponds with a water depth greater than $0.5\,\mathrm{m}$ belonged to the ASP class, which made up the largest proportion of ponds in the entire study area. Despite the wide range of water depths in the surveyed ponds the deeper ponds tended to be larger than the shallower ones which coincided with increased thaw depths beneath the deeper ponds. This tendency was especially pronounced for ponds with depths greater than $0.5\,\mathrm{m}$. In contrast, ISPs with water depths of less than $0.5\,\mathrm{m}$ did not show any clear depth-size correlation. The size of the ISPs appeared to be mainly determined by the size of the polygonal structures.

Ice cover growth (freezing) rates were investigated in three different ponds during the winters of 2010-2011 and 2011-2012. The freezing rate detection was limited to the first part of winter since temperature profile measurements were only available to a maximum depth of about $0.8\,\mathrm{m}$ (see Sect. 3.2). During the winter of 2010-2011 the average growth rate of the ice cover was $0.91 \pm 0.11\,\mathrm{cm\,d^{-1}}$ (Fig. 4a). The three investigated ponds showed deviations from the linear average of up to $0.15\,\mathrm{m}$, which were particularly evident from the beginning of October to the middle of November. The shallowest pond (ISP1) revealed the highest freezing rate and was completely frozen (to the bottom: a depth of about $0.4\,\mathrm{m}$) by the beginning of November. The other ponds (ASP1 and ASP2) achieved a similar ice cover thickness about three weeks later. In contrast to the winter of 2010-2011, all investigated ponds showed a very consistent rate of ice cover formation during the winter of 2011-2012 (Fig. 4b), when the average growth rate of the ice cover was $1.24 \pm 0.12\,\mathrm{cm\,d^{-1}}$ with only minor deviations from the linear average (up to about $0.05\,\mathrm{m}$, which is well within the assumed measurement uncertainty). Despite the linear character of the freezing process, the measurements showed some temporal variations in the freezing rate. During both winter periods pond ISP1 showed a very linear freezing behavior but, in contrast, the deeper ponds showed a lower rate of freezing at the beginning of the freezing period, a slightly increased rate in the middle of the period, and a lower rate again when the ice cover approached the bottom of the ponds.

4.2 Distribution of gas bubbles within the ice cover

Most of the ice columns were very clear with only a few visible bubbles. After a short warm event during the field campaign a very thin layer of white ice ($1-3\,\mathrm{cm}$ layer thickness) was observed above black ice at some locations. This white ice layer was excluded from further analysis. The ice columns from the ISP1 and ISP2 ponds showed a layer of abundant bubbles close to the bottom of the ponds, starting from a depth of about $15\,\mathrm{cm}$. Moss stems in the sediments on the floor of these two ponds were usually completely surrounded by bubbles. The diameter of these bubbles ranged from about $1\,\mathrm{mm}$ to $5\,\mathrm{mm}$. Ice samples containing these dense and often interconnected bubbles along moss stems were excluded from the CH_4 concentration measurements.

In addition, two or three thin layers of bubbles were observed in ISP1 and ISP2 at depths of between 5 and $15\,\mathrm{cm}$. Three very thin layers of bubbles were also observed at similar depths (between 5 and $15\,\mathrm{cm}$) in the ice columns from pond ISP3. The consistent occurrence of these thin bubble layers in similar depths and different ponds indicates a formation related to air pressure changes. The three ISPs feature similar water depths of 30 to $45\,\mathrm{cm}$ and we expect similar freezing rates. However, the sizes of these bubbles layers were assessed to be negligible compared to the ice sample sizes so that they were not excluded from the CH_4 concentration measurements. The ice columns from the relatively deep ponds (ASP1, ASP2, and ASP3), which had depths greater than $0.5\,\mathrm{m}$, did not reach the bottom of the ponds and hence the presence or absence of a layer of abundant bubbles close to the bottom of the ponds (as seen in the shallow ISP1 and ISP2 ponds) could not be verified. The ice columns from pond ASP3 revealed a narrow bubble layer at about $15\,\mathrm{cm}$ depth similar to that seen in the shallow ponds, but those from ponds ASP1 and ASP2 showed no visible bubbles between the surface and a depth of $35\,\mathrm{cm}$. However, all ice columns from the deep ponds were consistent in showing two to three thin bubble layers between depths of 35 and $40\,\mathrm{cm}$.

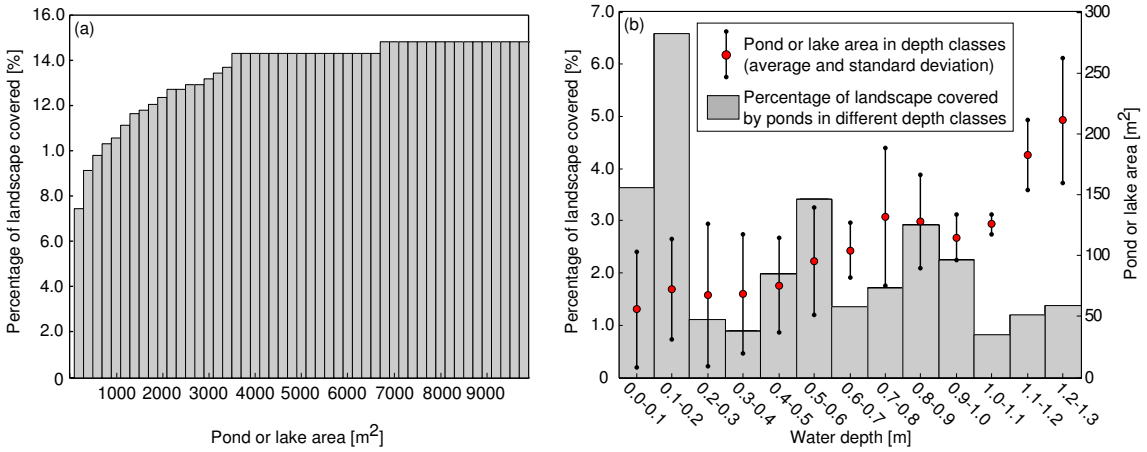

Fig. 3. Cumulative percentage of landscape covered by ponds in different size classes (a). Percentage of landscape covered by ponds in different depth classes (b). The secondary y-axis in (b) shows the average surface area for each depth class. The whiskers indicate the standard deviation for each depth class.

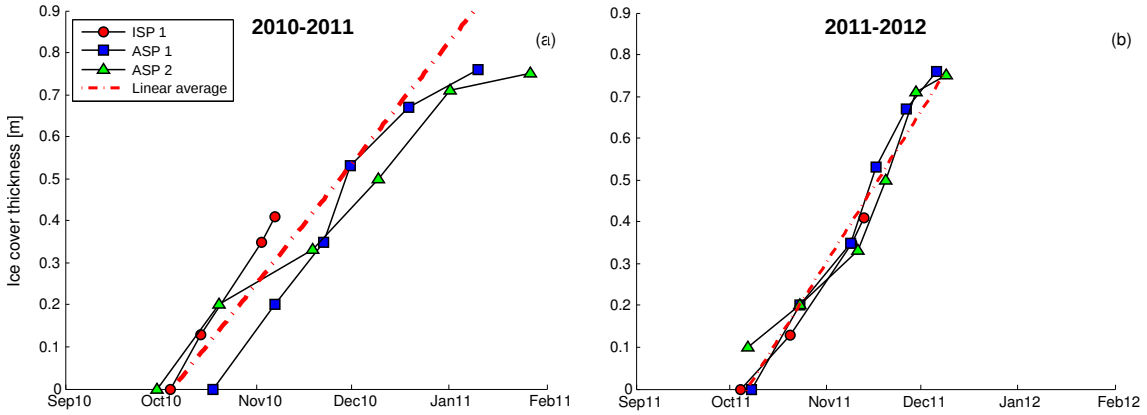

Fig. 4. Growth of ice cover inferred from water temperature measurements in three different ponds during (a) the winter of 2010-2011, and (b) the winter of 2011-2012.

4.3 Methane concentrations in lake and pond ice

The CH_4 concentrations obtained from all ice samples are shown in Figure 5, where they are plotted semi-logarithmically against the ratio of sample depth to maximum water depth. The whiskers following the orientation of the depth axis indicate the sample size while the whiskers following the orientation of the concentration axis indicate uncertainties in the measured CH_4 concentrations according to the Monte-Carlo simulations (see Sect. 3.3). In addition, the samples are color coded according to the surface area of the lake or pond from which they were obtained. The CH_4 concentration within the ice cover showed considerable variation, ranging from the detection limit of the gas analyzer up to $0.08\,\mathrm{mol\,m^{-3}}$. The detection limit of the used GC setup was at about $1\,\mathrm{ppm}$ which would equate to about $2\times10^{-5}\,\mathrm{mol\,m^{-3}}$ for CH_4 concentrations in ice samples assuming a head space volume of about $0.5\mathrm{l}$. On average about $2\times10^{-3}\,\mathrm{mol\,m^{-3}}$ ($0.03\,\mathrm{g_{CH_4}\,m^{-3}}$) was stored in the ice cover between the surface and a depth of $0.65\,\mathrm{m}$. However, these concentrations varied over two orders of magnitude indicating marked differences between the different waterbody types. The CH_4 concentration was generally observed to increase with depth. The highest CH_4 concentrations were recorded from waterbodies with surface areas of less than $50\,\mathrm{m^2}$ and in ice samples from close to the bottom of waterbodies. The results suggest an exponential relationship between CH_4 concentration and ice cover thickness; the measured concentrations generally followed an exponential trend, with the exception of four outliers. A detailed analysis of individual CH_4 profiles confirmed the exponential increase in CH_4 concentrations with depth and the

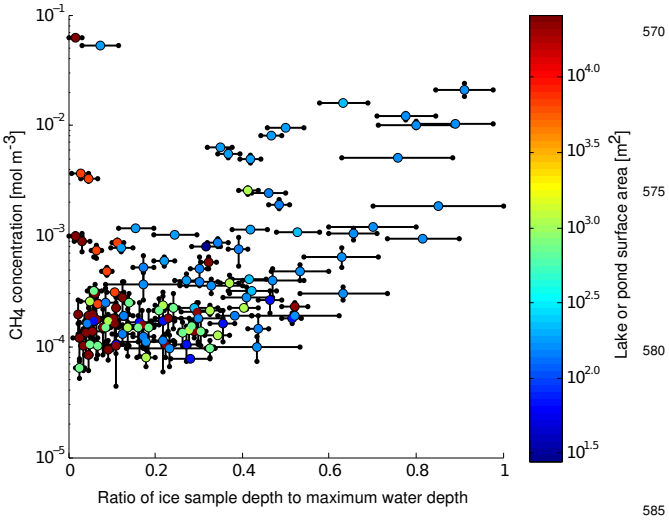

Fig. 5. Methane concentrations within the ice cover of different lakes and ponds, plotted against the ratio of sample depth to maximum water depth (note the logarithmic scale). The circles representing individual samples are colored according to the surface area of the lake or pond from which they came.

marked differences between waterbodies (see Fig. 6). An exponential increase in CH_4 concentration was recorded for all ponds in which the acquired ice columns reached close (about $30\,\mathrm{cm}$) to the bottom of the waterbody. The lowest CH_4 concentrations were recorded in the ice columns from large thermokarst lakes. In these lakes only the uppermost part of the ice cover was sampled relative to the maximum lake depths. Two of the four outliers that do not fit into the general exponential behavior revealed very high CH_4 concentrations of up to $0.08\,\mathrm{mol\,m^{-3}}$ (Fig. 5). The other two outliers only showed moderately increased concentrations of about $0.003\,\mathrm{mol\,m^{-3}}$. All outliers were found relatively close to the top of the ice cover and three of four outliers were observed at thermokarst lakes with surface areas larger than $10^4\,\mathrm{m^2}$.

4.4 Modeling methane storage in the ice cover

The maximum CH_4 concentrations measured in the ISP1, ISP3, and ASP3 samples were about one order of magnitude higher than those from ISP2, ASP1, ASP2, and ASP4 (Fig. 6). The ice samples were typically 5 to $10\,\mathrm{cm}$ high which placed a limit on the depth resolution, but this was improved to some extent by overlap between samples. The uncertainty in the CH_4 concentration from each sample was relatively low although some differences were observed between overlapping samples, especially in those from the ASP1 and ASP2 ponds. Despite these uncertainties and the limited depth resolution all ponds consistently revealed an exponential increase in CH_4 concentration with depth (Fig. 6). The ASP3 profile in particular showed a very sharp increase in concentration in the deepest sample. The increase in CH_4 concentrations in the ISP1 and ISP2 coincided with increased bubble densities, but no general relationship was observed between bubble density and CH_4 concentration in the ISP3, ASP1, ASP2, and ASP3 ponds.

The derived CH_4 concentration profiles for six of the ponds were analyzed and the mass balance model fitted to these profiles in order to estimate net CH_4 production rates (see. Sect. 3.4). From this fitting procedure the effective bubble cross-sections and net CH_4 production rates were obtained for all the analyzed ponds, and also for an additional ASP (ASP4). The model was able to reproduce the observed CH_4 concentration profiles for all of the ponds. The best fit results and the 95% confidence intervals of the fitting procedure are shown in Figure 6. Most of the differences between the best fit and the actual measurements fall within the 95% confidence interval of the model output, taking into account the depth resolution and the uncertainties in the measured CH_4 concentrations. The model also successfully reproduced the sharp increase in CH_4 concentration noted in the ASP3 profile. In this particular case the model simulated the storage of excess CH_4 in the ice cover, since the maximum solubility of CH_4 in water (about $2.5\,\mathrm{mol\,m^{-3}}$ at about $0^\circ\,\mathrm{C}$ and $1000\,\mathrm{hPa}$) was reached in the shrinking water column.

The inferred net CH_4 production rates resulting from the fitting procedure revealed marked variations in net CH_4 production between the different waterbodies (Fig. 7). The net production rates ranged from 10^{-11} to $10^{-7}\,\mathrm{mol\,m^{-2}\,s^{-1}}$ (0.01 to $140\,\mathrm{mg_{CH_4}\,m^{-2}\,d^{-1}}$) and the effective bubble cross-sections ranged from $10^{-4}\,\mathrm{m}$ to $10^{-2}\,\mathrm{m}$. The net CH_4 production rate was generally higher in profiles with smaller effective bubble cross-sections. The highest net CH_4 production rates were calculated for the ASP1, ASP2, ASP3, and ASP4 which had maximum water depths greater than $0.5\,\mathrm{m}$ and showed clear signs of recent permafrost degradation. In contrast, lower net CH_4 production rates but larger bubble cross-sections were calculated for the ISP1, ISP2, and ISP3.

5 Discussion

5.1 Characteristics and sensitivities of Arctic ponds

The survey of ponds and lakes within the study area clearly showed an abundance of ponds in the lowland tundra landscape of the Lena River Delta. Almost 10% of the total land surface was occupied by waterbodies with surface areas of less than $300\,\mathrm{m^2}$, most of which were no deeper than $1\,\mathrm{m}$. The abundance of small waterbodies in the Arctic has been noted in a number of previous studies (Emmerton et al., 2007; Grosse et al., 2008).

Furthermore, this study has demonstrated that the freezing rates of ponds can vary greatly from one pond to another, and from one year to another. Ice thicknesses measurements

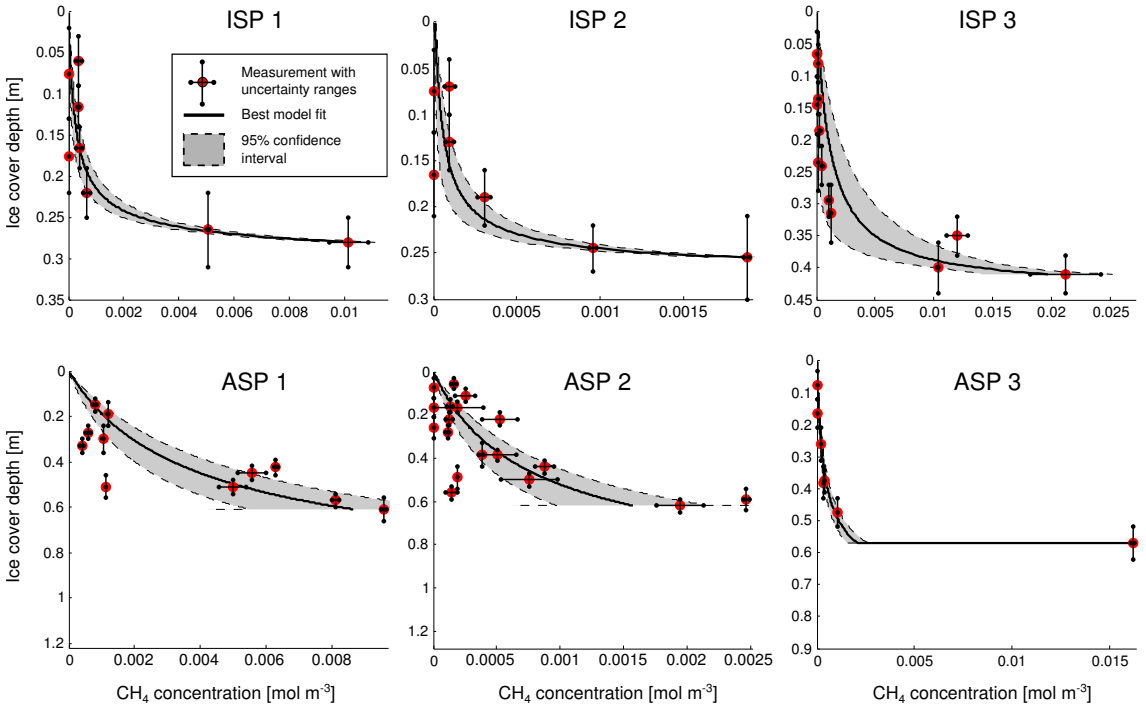

Fig. 6. Measured and modeled CH_4 concentrations with ice cover depth of different ponds. The whiskers show the measurement uncertainty and the shaded areas indicate the 95% confidence interval of the model. The range of depth axis represents the maximum pond depth. Sampling was limited to a maximum ice cover depth of about 60 cm due to the length of the used guide bar of the chainsaw.

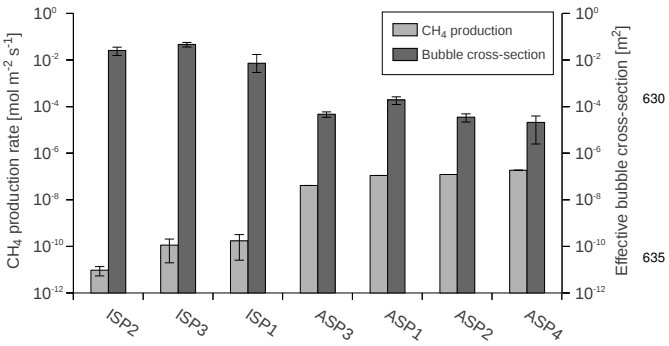

Fig. 7. Net methane production and effective bubble cross-section for different ponds, calculated by inverse modeling using the 1D mass balance model (note the logarithmic scale). The whiskers indicate the 95% confidence interval of the model results.

from two consecutive years revealed a difference in ice cover thickness of about 40%. Detailed investigations of the surface energy balance within the study area have suggested that marked interannual differences in the freezing rate can be largely attributed to differences in the snow cover and the wintertime cloud cover (Langer et al., 2011b).

The survey of waterbodies also revealed that a large fraction of ponds are no deeper than 20 cm. These shallow ponds occur mainly in low-centered polygons with little or no signs of degradation. The occurrence and size of such ponds is assumed to be directly related to the polygonal microtopography, which also explains why no relationship could be observed between pond size and water depth. There is a clear contrast with the frequency of ponds deeper than 0.5 m. These ponds show a more uniform depth distribution with a slight maximum between 0.5 and 1 m. A depth-size relationship was observed for these deeper ponds. The existence of such a relationship suggests a link between the erosive processes leading to the deepening of the pond and the size of the waterbody. However, the poorly defined depth-size relationships indicates a rather complex interrelationship.

5.2 CH_4 concentrations and net production rates

All of the CH_4 profiles derived from ice samples indicate an exponential increase in CH_4 concentration with depth, which is in agreement with previous observations by Phelps et al. (1998) from various Alaskan and Canadian lakes. The consistency between these two studies suggests that both freeze-degassing of CH_4 and CH_4 storage within the ice cover generally occurs in shallow lakes. Some individual concentrations have been observed to deviate from the general exponential behavior. These outliers may be explained by the ad-

mixture of ebullition bubbles, which are not explicitly accounted for in this study. However, the exponential relationship between ice depth and CH_4 concentration can be reproduced by a simplified mass balance model, assuming constant net CH_4 production and bubble accumulation. The exponential shape results from the dynamic balance between net CH_4 production, freeze-degassing, and storage of CH_4 within the ice cover.

The mass balance model was successfully fitted to the measured CH_4 concentrations by optimizing the net CH_4 production rate and the effective bubble size. A high level of confidence was achieved in all profiles. Furthermore, the model was able to realistically reproduce the sharp increase in CH_4 concentration observed in one of the profiles. This indicated that the model was able to accurately represent the timing of CH_4 saturation in the shrinking water column during freezing. The overall high level of performance of the model for the different profiles suggests that the basic process of CH_4 freeze-degassing and storage in the ice cover is adequately represented. In addition, sensitivity tests revealed that the fit was very robust against variations in the initial values of net CH_4 production and effective bubble size. This inspires confidence that the magnitudes of the fitted net CH_4 production and bubble accumulation rates are realistic. The results were also found to be very robust against uncertainties in the initial CH_4 concentration within the water column, prior to the onset of freezing. Except for the ponds ISP2 and ASP2, sensitivity tests over the entire range of possible initial CH_4 concentrations (1×10^{-9} and $1 \times 10^{-5}\,\mathrm{mol\,m^{-3}}$ see Sect. 3.4) were not found to affected the modeled magnitudes of CH_4 production and effective bubble cross-section. For the ponds ISP2 and ASP2 the model produced consistent results with initial CH_4 concentrations ranging between 1×10^{-9} and $1 \times 10^{-7}\,\mathrm{mol\,m^{-3}}$. This limited range relates to the generally very low CH_4 concentrations found in these ponds. Higher initial CH_4 concentrations would require methane decomposition instead of production to reproduce the observed CH_4 concentration profiles. Despite the robustness of the model, unpredictable errors due to gas loss from the edges of the samples or methane oxidation within the ice could negatively bias the measured concentration rates, and consequently the resulting net CH_4 production rates. Oversimplified model assumptions, such as uniformly distributed CH_4 concentrations and a constant rate of bubble accumulation, could also affect the simulated net CH_4 production rates. The model results must therefore be considered to represent first order estimates. The results of the fitting procedure generally suggest marked differences in the net CH_4 production from different pond types. Initial state ponds (water $\mathrm{depth} < 0.5\,\mathrm{m}$) show very low net production rates, of the order of 10^{-11} and $10^{-10}\,\mathrm{mol\,m^{-2}\,s^{-1}}$ (0.01 to $0.14\,\mathrm{mg_{CH_4}\,m^{-2}\,d^{-1}}$). In contrast, advanced state ponds ($\mathrm{depth} > 0.5\,\mathrm{m}$) with clear signs of thermal erosion show net CH_4 production rates of the order of $10^{-7}\,\mathrm{mol\,m^{-2}\,s^{-1}}$ ($140\,\mathrm{mg_{CH_4}\,m^{-2}\,d^{-1}}$). Similar ranges of CH_4 emission rates have previously been reported in summer from ponds in a similar type of landscape on Bylot Island, Canada (Laurion et al., 2010). The net CH_4 production rates from the ponds at our study area were of a similar magnitude to observed summertime CH_4 emission rates (excluding ebullition) from ice-wedge ponds on Bylot Island. In addition, the results of this study provide further evidence that the marked differences in net CH_4 production rates between the different pond types are likely to be due to fundamental differences in biogeochemical processes resulting from active thermal erosion which increases the availability of organic material (Laurion et al., 2010; Laurion and Mladenov, 2013).

The differences in net CH_4 production may also be related to differences in the vegetation growing on the bottom of the ponds such as *Scorpidium scorpioides*. These mosses live in symbiosis with CH_4-oxidizing bacteria that could effectively limit CH_4 emission (Liebner et al., 2011). Photosynthesis and oxygen production are still possible beneath the growing ice cover during early winter. Indicators of active photosynthesis in ISPs during freezing is provided by the large number of bubbles observed around moss stems. However, other processes such as CO_2 emission through moss respiration or preferential bubble nucleation at the moss stems could have contribute to the formation of these bubble clusters. Since it was likely that the ice samples from these highly porous layers have lost their original gas content during sampling, they were excluded from the CH_4 concentration measurements. Thus, the impact of mosses on the net CH_4 production and storage in the ice cover remains unclear.

The maximum summertime CH_4 emission rates per square meter from the average tundra landscape on Samoylov Island are of the order of $5 \times 10^{-8}\,\mathrm{mol\,m^{-2}\,s^{-1}}$ ($60\,\mathrm{mg_{CH_4}\,m^{-2}\,d^{-1}}$) (Sachs et al., 2008; Wille et al., 2008). These average landscape CH_4 emission rates were obtained by eddy covariance measurements with typical footprint areas of several hundreds of square meters including ponds and vegetated tundra soils. Thus, these measurements are not directly comparable to the production rates of individual ponds inferred by this study. Nevertheless, the eddy covariance measurements provide a reference value which allows to asses the strength of CH_4 production in ponds relative to a landscape scale CH_4 emission rate. Under this consideration, the early winter net CH_4 production rates per square meter from ASPs are about five times larger than the maximum summertime landscape scale CH_4 emissions per square meter. Considering that ponds occupy about 10% of the tundra landscape, this stresses the importance of ponds and the freezing period to the local carbon cycle. Even during the freezing period small waterbodies can be hotspots of CH_4 production in a tundra landscape. It is, however, important to note that our results do not take into account CH_4 that is transported and stored in the ice cover through ebullition, and the total CH_4 production from ASPs is therefore likely to be much greater than our modeling suggests.

6 Conclusions

Our results show that ponds in the polygonal tundra can be important sources of CH_4 during the freezing period. Extensive measurements in the ice cover of different ponds have revealed that the CH_4 concentrations increase exponentially with depth, indicating intensive CH_4 production under the growing ice cover. The measured CH_4 concentration profiles were successfully reproduced by 1D mass balance model demonstrating that the exponential shape results from the dynamic balance between net CH_4 production, freeze-degassing, and storage of CH_4 within the ice cover. Furthermore, inverse modeling has revealed high net CH_4 production rates in ponds showing signs of erosion in the surrounding polygonal ground structures, which contrasts with the low net production rates observed in ponds located within almost intact polygonal ground structures. These results have far ranging implications for the CH_4 emission potential of lowland tundra landscapes, since:

- The CH_4 that is produced during the freezing period is likely to be released into the atmosphere during the spring melt.
- Ponds are abundant in lowland tundra landscapes and their occurrence is closely related to the state of degradation of surface structures in permafrost landscapes. Hence, further degradation of surface structures due to thawing permafrost may affect the occurrence of ponds and thus the CH_4 emissions from tundra landscapes.
- The net production of CH_4 from ponds that show signs of erosion in the surrounding polygonal ground structures is observed to be two to three orders of magnitude greater than from ponds located within largely intact permafrost. Any future warming-induced erosion and pond expansion may therefore greatly increase the CH_4 emission potential of tundra landscapes.

Appendix A

The mass balance of methane in a freezing pond can be written as

$$\mathrm{N_i} + \mathrm{N_g} + \mathrm{N_a} - \mathrm{N_0} - \mathrm{N_P} = 0, \tag{A1}$$

where $\mathrm{N_i}$ is the amount of CH_4 molecules that are stored in the ice cover, $\mathrm{N_g}$ is the amount of methane stored in bubbles at the ice-water interface, $\mathrm{N_a}$ is the number of dissolved methane molecules in the water column, $\mathrm{N_0}$ is the amount of dissolved methane that is stored in the water column at the start of freezing, and $\mathrm{N_P}$ is the number of CH_4 molecules produced. The individual CH_4 components of the mass balance are parameterized as

$$\mathrm{N_i} = \mathrm{A_b} \int_0^t \mathrm{C}(\tau)\, \frac{\partial \mathrm{z}(\tau)}{\partial \tau}\, d\tau, \tag{A2}$$

$$\mathrm{N_g} = \mathrm{C}(t)\, \mathrm{V_b}, \tag{A3}$$

$$\mathrm{N_a} = \mathrm{C}(t)\, \mathrm{k_H}\, \mathrm{R}\, \mathrm{T_w}\, (\mathrm{z_0} - \mathrm{z}(t)), \tag{A4}$$

$$\mathrm{N_0} = \mathrm{C_0}\, \mathrm{z_0}, \tag{A5}$$

$$\mathrm{N_P} = \int_0^t \mathrm{P}(\tau)\, d\tau, \tag{A6}$$

where $\mathrm{C}(t)$ is the concentration of methane in bubbles at the ice-water interface at time t; $\mathrm{k_H}$ is the Henry's law constant of methane, assuming constant pressure and a water temperature $\mathrm{T_w}$ of $273.15\,\mathrm{K}$; R is the universal gas constant; $\mathrm{A_b}$ is the effective bubble size in direct contact with the ice-water interface; $\mathrm{z}(t)$ is the ice cover thickness; $\mathrm{V_b}$ is the effective volume of bubbles at the ice-water interface; $\mathrm{z_0}$ is the depth of the water column at the start of freezing; $\mathrm{C_0}$ is the concentration of methane in water at the start of freezing; and P is the rate of net methane production in the pond. Equation A4 is modified to

$$\mathrm{N_a} = \mathrm{k_H}\, (\mathrm{z_0} - \mathrm{z}(t)), \tag{A7}$$

as soon as CH_4 saturation is reached in the remaining water column so that all excess methane is deposited directly into the ice cover. Thus, combining the equations A1 - A7 results in two first order linear differential equations for (i) the duration of CH_4 under-saturation ($t \leq \mathrm{t_S}$) and (ii) the period of CH_4 saturation ($t > \mathrm{t_S}$)

$$\begin{cases} a\,\mathrm{C}(t) + b\,\frac{\partial \mathrm{C}(t)}{\partial t} - \mathrm{P}(t) = 0, & \text{for } 0 \leq t \leq \mathrm{t_S} \\ c\,\mathrm{C}(t) + d\,\frac{\partial \mathrm{C}(t)}{\partial t} - e - \mathrm{P}(t) = 0, & \text{for } t > \mathrm{t_S} \end{cases}, \tag{A8}$$

where a, b, c, d, and e summarize the parameters according to equations A2 - A7. The differential equations can be solved with exponential functions so that the concentration of methane in the water column and in the ice cover can be calculated for each time step in the freezing process.

Acknowledgements. Special thanks go to Katrin Fröb and Karoline Morling for their invaluable work in the field and laboratory. Furthermore, we thank Waldemar Schneider and our Russian partners at AARI and the Lena Delta Reserve for the logistical support of our field work. We gratefully acknowledge the financial support by the Helmholtz Association through a grant (VH-NG 203) awarded to Julia Boike. Furthermore, the authors acknowledge the financial support by the European Union FP7-ENV project PAGE21 under contract number GA282700. We also like to thank the two anonymous reviewer for the very constructive comments which helped to improve our manuscript. Moreover, we like to thank the associate editor Isabelle Laurion for very helpful comments and suggestions.

References

Abnizova, A., Siemens, J., Langer, M., Boike, J., 2012. Small ponds with major impact: The relevance of ponds and lakes in permafrost landscapes to carbon dioxide emissions. Global Biogeochemical Cycles 26 (2), GB2041.

Anderson, G., 1976. Error propagation by the Monte Carlo method in geochemical calculations. Geochimica et Cosmochimica Acta 40 (12), 1533–1538.

Boereboom, T., Depoorter, M., Coppens, S., Tison, J.-L., 2012. Gas properties of winter lake ice in Northern Sweden: implication for carbon gas release. Biogeosciences 9 (2), 827–838.

Boike, J., Kattenstroth, B., Abramova, K., Bornemann, N., Chetverova, A., Fedorova, I., Fröb, K., Grigoriev, M., Grüber, M., Kutzbach, L., Langer, M., Minke, M., Muster, S., Piel, K., Pfeiffer, E.-M., Stoof, G., Westermann, S., Wischnewski, K., Wille, C., Hubberten, H.-W., 2013. Baseline characteristics of climate, permafrost and land cover from a new permafrost observatory in the Lena River Delta, Siberia (1998–2011). Biogeosciences 10 (3), 2105–2128.

Boike, J., Langer, M., Lantuit, H., Muster, S., Roth, K., Sachs, T., Overduin, P., Westermann, S., McGuire, A., 2012. Permafrost – Physical Aspects, Carbon Cycling, Databases and Uncertainties. Springer Netherlands, pp. 159–185.

Brosius, L. S., Walter Anthony, K. M., Grosse, G., Chanton, J. P., Farquharson, L. M., Overduin, P. P., Meyer, H., 2012. Using the deuterium isotope composition of permafrost meltwater to constrain thermokarst lake contributions to atmospheric CH4 during the last deglaciation. Journal of Geophysical Research: Biogeosciences 117 (G1), G01022.

Brown, J., Ferrians Jr, O., Heginbottom, J., Melnikov, E., 1997. Circum-Arctic map of permafrost and ground-ice conditions. US Geological Survey Circum-Pacific Map.

Carte, A., 1961. Air bubbles in ice. Proceedings of the Physical Society 77 (3), 757–768.

Cole, J., Prairie, Y., Caraco, N., McDowell, W., Tranvik, L., Striegl, R., Duarte, C., Kortelainen, P., Downing, J., Middelburg, J., Melack, J., 2007. Plumbing the Global Carbon Cycle: Integrating Inland Waters into the Terrestrial Carbon Budget. Ecosystems 10 (1), 172–185.

Craig, H., Wharton, R., McKay, C., 1992. Oxygen supersaturation in ice-covered Antarctic lakes: Biological versus physical contributions. Science 255 (5042), 318–321.

Emmerton, C. A., Lesack, L. F. W., Marsh, P., 2007. Lake abundance, potential water storage, and habitat distribution in the Mackenzie River Delta, western Canadian Arctic. Water Resources Research 43 (5), W05419.

Grigoriev, N., 1960. The temperature of permafrost in the Lena delta basin – deposit conditions and properties of the permafrost in Yakutia, 97–101In Russian.

Grosse, G., Romanovsky, V., Walter, K., Morgenstern, A., Lantuit, H., Zimov, S., 2008. Distribution of thermokarst lakes and ponds at three yedoma sites in Siberia. In: Proceedings of the 9th International Conference on Permafrost, Fairbanks, Alaska, 29 June–3 July 2008 . pp. 551–556.

Helbig, M., Boike, J., Langer, M., Schreiber, P., Runkle, B. R., Kutzbach, L., 2013. Spatial and seasonal variability of polygonal tundra water balance: Lena River Delta, northern Siberia (Russia). Hydrogeology Journal 21 (1), 133–147.

Hugelius, G., Tarnocai, C., Broll, G., Canadell, J., Kuhry, P., Swanson, D., 2013. The Northern Circumpolar Soil Carbon Database: spatially distributed datasets of soil coverage and soil carbon storage in the northern permafrost regions. Earth System Science Data 5, 3–13.

Karlsson, J., Giesler, R., Persson, J., Lundin, E., 2013. High emission of carbon dioxide and methane during ice thaw in high latitude lakes. Geophysical Research Letters 40, 1123–1127.

Killawee, J., Fairchild, I., Tison, J.-L., Janssens, L., Lorrain, R., 1998. Segregation of solutes and gases in experimental freezing of dilute solutions: Implications for natural glacial systems. Geochimica et Cosmochimica Acta 62 (23), 3637–3655.

Koven, C. D., Ringeval, B., Friedlingstein, P., Ciais, P., Cadule, P., Khvorostyanov, D., Krinner, G., Tarnocai, C., 2011. Permafrost carbon-climate feedbacks accelerate global warming. Proceedings of the National Academy of Sciences 108 (36), 14769–14774.

Kutzbach, L., Wagner, D., Pfeiffer, E., 2004. Effect of microrelief and vegetation on methane emission from wet polygonal tundra, Lena Delta, Northern Siberia. Biogeochemistry 69 (3), 341–362.

Kutzbach, L., Wille, C., Pfeiffer, E.-M., 2007. The exchange of carbon dioxide between wet arctic tundra and the atmosphere at the Lena River Delta, Northern Siberia. Biogeosciences 4 (5), 869–890.

Lachenbruch, A. H., 1962. Mechanics of thermal contraction cracks and ice-wedge polygons in permafrost. Geological Society of America Special Papers 70, 1–66.

Langer, M., Westermann, S., Muster, S., Piel, K., Boike, J., 2011a. The surface energy balance of a polygonal tundra site in northern Siberia – Part 1: Spring to fall. The Cryosphere 5 (1), 151–171.

Langer, M., Westermann, S., Muster, S., Piel, K., Boike, J., 2011b. The surface energy balance of a polygonal tundra site in northern Siberia – Part 2: Winter. The Cryosphere 5 (2), 509–524.

Laurion, I., Mladenov, N., 2013. Dissolved organic matter photolysis in Canadian arctic thaw ponds. Environmental Research Letters 8 (3), 035026–35037.

Laurion, I., Vincent, W. F., MacIntyre, S., Retamal, L., Dupont, C., Francus, P., Pienitz, R., 2010. Variability in greenhouse gas emissions from permafrost thaw ponds. Limnology and Oceanography 55 (1), 115–133.

Liebner, S., Zeyer, J., Wagner, D., Schubert, C., Pfeiffer, E.-M., Knoblauch, C., 2011. Methane oxidation associated with submerged brown mosses reduces methane emissions from Siberian polygonal tundra. Journal of Ecology 99 (4), 914–922.

Lipp, G., Körber, C., Englich, S., Hartmann, U., Rau, G., 1987. Investigation of the behavior of dissolved gases during freezing. Cryobiology 24 (6), 489–503.

McGuire, A. D., Anderson, L. G., Christensen, T. R., Dallimore, S., Guo, L., Hayes, D. J., Heimann, M., Lorenson, T. D., Macdonald, R. W., Roulet, N., 2009. Sensitivity of the carbon cycle in the Arctic to climate change. Ecological Monographs 79 (4), 523–555.

Morgenstern, A., Ulrich, M., Günther, F., Roessler, S., Fedorova, I. V., Rudaya, N. A., Wetterich, S., Boike, J., Schirrmeister, L., 2013. Evolution of thermokarst in East Siberian ice-rich permafrost: A case study. Geomorphology 201, 363–379.

Muster, S., Heim, B., Abnizova, A., Boike, J., 2013. Water body distributions across scales: a remote sensing based comparison of three arctic tundra wetlands. Remote Sensing. 2013; 5 (4):-.

5 (4), 1498–1523.

Muster, S., Langer, M., Heim, B., Westermann, S., Boike, J., 2012. Subpixel heterogeneity of ice-wedge polygonal tundra: a multi-scale analysis of land cover and evapotranspiration in the Lena River Delta, Siberia. Tellus B 64, 1–19.

Negandhi, K., Laurion, I., Whiticar, M. J., Galand, P. E., Xu, X., Lovejoy, C., 2013. Small Thaw Ponds: An Unaccounted Source of Methane in the Canadian High Arctic. PLoS ONE 8 (11), e78204.

O'Connor, F. M., Boucher, O., Gedney, N., Jones, C. D., Folberth, G. A., Coppell, R., Friedlingstein, P., Collins, W. J., Chappellaz, J., Ridley, J., Johnson, C. E., 2010. Possible role of wetlands, permafrost, and methane hydrates in the methane cycle under future climate change: A review. Reviews of Geophysics 48 (4), RG4005.

Phelps, A. R., Peterson, K. M., Jeffries, M. O., 1998. Methane efflux from high-latitude lakes during spring ice melt. Journal of Geophysical Research: Atmospheres (1984–2012) 103 (D22), 29029–29036.

Sachs, T., Wille, C., Boike, J., Kutzbach, L., 2008. Environmental controls on ecosystem-scale CH4 emission from polygonal tundra in the Lena River Delta, Siberia. Journal of Geophysical Research: Biogeosciences 113 (G3), G00A03.

Van Hulzen, J., Segers, R., Van Bodegom, P., Leffelaar, P., 1999. Temperature effects on soil methane production: an explanation for observed variability. Soil biology and biochemistry 31 (14), 1919–1929.

Walter, K., Zimov, S., Chanton, J., Verbyla, D., Chapin, F., 2006. Methane bubbling from Siberian thaw lakes as a positive feedback to climate warming. Nature 443 (7107), 71–75.

Walter Anthony, K. M., Anthony, P., 2013. Constraining spatial variability of methane ebullition seeps in thermokarst lakes using point process models. Journal of Geophysical Research: Biogeosciences 118 (3), 1015–1034.

Walter Anthony, K. M., Vas, D. A., Brosius, L., Chapin III, F., Zimov, S. A., Zhuang, Q., 2010. Estimating methane emissions from northern lakes using ice-bubble surveys. Limnol. Oceanogr.: Methods 8, 592–609.

Wei, P., Huang, C., Lee, K., 2003. Nucleation of bubbles on a solidification front—experiment and analysis. Metallurgical and Materials Transactions B 34 (3), 321–332.

Wetterich, S., Schirrmeister, L., Meyer, H., Viehberg, F. A., Mackensen, A., 2008. Arctic freshwater ostracods from modern periglacial environments in the Lena River Delta (Siberian Arctic, Russia): geochemical applications for palaeoenvironmental reconstructions. Journal of Paleolimnology 39 (4), 427–449.

Wik, M., Crill, P. M., Bastviken, D., Danielsson, Å., Norbäck, E., 2011. Bubbles trapped in arctic lake ice: Potential implications for methane emissions. Journal of Geophysical Research: Biogeosciences 116 (G3), G03044.

Wille, C., Kutzbach, L., Sachs, T., Wagner, D., Peiffer, E., 2008. Methane emission from Siberian arctic polygonal tundra: eddy covariance measurements and modeling. Global Change Biology 14 (6), 1395–1408.

Yoshimura, K., Inada, T., Koyama, S., 2008. Growth of spherical and cylindrical oxygen bubbles at an ice- water interface. Crystal Growth and Design 8 (7), 2108–2115.

Zimov, S., Voropaev, Y. V., Semiletov, I., Davidov, S., Prosiannikov, S., Chapin, F. S., Chapin, M., Trumbore, S., Tyler, S., 1997. North Siberian lakes: A methane source fueled by Pleistocene carbon. Science 277 (5327), 800–802.

Zubrzycki, S., Kutzbach, L., Grosse, G., Desyatkin, A., Pfeiffer, E., 2013. Organic carbon and total nitrogen stocks in soils of the Lena River Delta. Biogeosciences 10 (6), 3507–3524.